

Large-Scale Daylight Photoluminescence: Automated Photovoltaic Module Operating Point Detection and Performance Loss Assessment by Quantitative Signal Analysis

Lukas Koester,* Atse Louwen, Sascha Lindig, Giampaolo Manzolini, and David Moser

Daylight photoluminescence (DPL) is a relatively novel imaging technique utilized in photovoltaic (PV) system inspection, using the sun as excitation source. Filtering the luminescence signal from the strong sun irradiation is its main challenge. Images acquired at two different operating points (OPs) of the module, allow subtraction of the background radiation while maintaining the luminescence signal. A DPL-ready inverter, which is able to toggle between manually selectable OPs of connected PV modules, is presented in this work. Synchronization of image acquisition and OP switching becomes particularly challenging if the camera is applied to unmanned aerial vehicles. To overcome this challenge, an algorithm is developed to identify OP switches in a set of images taken in the field by investigating image intensities. Further, by working out the detailed dependencies of the signal recorded during DPL, the temperature coefficient of photoluminescence intensity is derived theoretically, and its impact on quantitative inspections. The potential field application of DPL images to identify performance loss in PV modules is investigated by two approaches: recording the signal intensity of images over time and comparing the signal intensity of different PV modules in one image. For both approaches, their hypothetical applicability is shown experimentally.

1. Introduction

During operation and maintenance (O&M) of photovoltaic (PV) power plants, one important task is inspection of PV modules to detect a variety of issues that can affect their power production or safety. The most commonly used ones to inspect PV modules are visual and infrared (IR) inspection. These methods are quick and cheap to apply, but do allow only for a limited insight into possible issues and defects. For instance, IR is used to detect hot spots which can evolve due to a variety of defects. Often, the root cause of hot spots cannot be determined using visual inspection or IR.

Luminescence techniques such as electroluminescence (EL) and daylight photoluminescence (DPL) provide much higher detail in inspecting PV modules, allowing more defects to be identified and differentiated. Therefore, the technical standard IEC 62446-3:2017^[1] on outdoor IR thermography suggests to identify the root


causes of hot spots with EL imagery. EL works by injecting a forward current into the PV module,^[2] which triggers recombination processes resulting in the emission of a luminescence signal in the short-wave infrared regime (SWIR). Hence, to perform EL inspection, it is necessary to disrupt the electrical connection of PV module strings. This problem can be overcome by using EL-ready inverters which are able to directly inject power from the grid into the connected PV module strings.^[3] EL-ready inverters are still being developed and are not common practice. Because of that, EL inspections applied today are much more costly in comparison to IR. Current guidelines for PV O&M suggest annual IR checks of the whole PV plant and to additionally verify anomalies using EL.^[4]

To increase throughput, and thereby overcome this cost barrier, EL inspections are applied using unmanned aerial vehicles (UAVs).^[5] A challenge is to receive high-quality images from a moving device. Therefore, it is necessary to work with short exposure times. Cameras with indium gallium arsenide (InGaAs) sensors allow exposure times of as little as 1 ms due to their high quantum efficiency in the SWIR and due to reduced thermal

L. Koester, A. Louwen, S. Lindig, D. Moser
Eurac Research
Institute for Renewable Energy
Viale Druso 1, 39100 Bolzano, Italy
E-mail: lukas.koester@eurac.edu

L. Koester, G. Manzolini
Dipartimento di energia
Politecnico di Milano
Via Lambruschini, 4, 20156 Milano, Italy

S. Lindig
Univers GmbH
Leopoldstraße 248, 80807 Munich, Germany

 The ORCID identification number(s) for the author(s) of this article can be found under <https://doi.org/10.1002/solr.202300676>.

© 2023 The Authors. Solar RRL published by Wiley-VCH GmbH. This is an open access article under the terms of the Creative Commons Attribution-NonCommercial-NoDerivs License, which permits use and distribution in any medium, provided the original work is properly cited, the use is non-commercial and no modifications or adaptations are made.

DOI: 10.1002/solr.202300676

noise at elevated temperatures. As a drawback, InGaAs sensors come with a relatively low resolution (around 1 megapixel) compared to silicon (Si) sensors.

A further development in luminescence imaging for PV plant inspections is the DPL method. Instead of injecting current, daylight is used as an excitation source. If the PV module is in open circuit (OC) conditions, carriers created in the PV module's silicon layer will recombine and partly emit a luminescence signal. To detect the small signal within the strong sunlight, a background image without a luminescence signal is taken and subtracted from the first one. The luminescence signal emission is avoided by setting the PV module into a high current (HC) state, where the carriers participate in the current flow and recombination is minimized. To avoid strong variation in the sunlight conditions, images of these two operating points (OPs) must be taken within a short time interval, and to decrease noise, several images of each OP must be taken and averaged. Different methods were developed to switch between the two different OPs of a PV module.^[6–9] In this work, a DPL-ready inverter, developed within H2020 project *TRUST-PV*, is presented, which enables toggling between OPs of the connected PV strings through preset parameters, without additional equipment or interference with the electrical layout of the PV plant. With the aspiration of using DPL from a UAV, semibatched imaging with subsequent automatic detection of recorded OP is developed to overcome synchronization issues between camera and inverter.

The luminescence signal depends on several aspects, but primarily the cell voltage and operating temperature. Therefore, a decrease in performance of the PV module and its cells over time should theoretically be visible in the luminescence intensity, given that the performance decrease is driven, at least partially, by a decrease in voltage. The challenge is to compare two measurements taken outdoors under different conditions. In the first step, parameters that impact the recorded signal must be defined. Then, two approaches are possible to identify performance decrease with DPL: First, the possibility of recognizing intensity losses in DPL images over a longer time period, which can be correlated to performance variations in PV modules. The feasibility of this method is tested in the presented work, by taking several DPL images within a short time frame, in which no degradation is expected, and assess if the same signal can be repeated. The second method to identify single PV modules with performance degradation is by comparing the DPL intensity of different PV modules in the same picture. This is done here by recording in one image frame DPL images with three PV modules of the same type, but with different OC voltage, identified by in-field current–voltage (IV) curve measurements.

The work is structured as follows: Section 2 provides a detailed introduction to the state of DPL imaging, and introduces the developed DPL-ready inverter as well as the camera used. In Section 3, the semibatched imaging method is introduced and the automated OP detection is outlined. Section 4 sheds light on DPL intensity, its temperature dependency, and describes the two approaches of how performance loss detection is investigated using DPL. The results of investigating performance decreases with DPL are given in Section 5 and 6 summarizes the work and gives an outlook on applying the presented methods.

2. Hardware

An image taken at OC conditions includes the luminescence signal, but when a PV module is irradiated by the sun, luminescence accounts for only around 3% of the total captured signal.^[6] A second image, captured at HC state within a short time frame, shows the same parameters but is missing the luminescence signal. Therefore, the HC image serves as a background image for subtraction. In fact, subtraction of the HC from the OC image (pixel-wise subtraction of intensity) results in the DPL image. In practice, several images must be acquired of each OP to increase the signal-to-noise ratio.

2.1. State of the Art of OP Switching

The first introduction of a practical DPL method was given in 2014 by Stoicescu et al.^[10] using an electrical device, which is included in the PV module string. The first method of DPL, which avoids any interference with the electrical string, was presented in 2018 by Bhoopathy et al.^[6] using a light-emitting diode (LED) array to cover one cell of a PV module and by this forcing the corresponding cell string of the PV module into OC conditions. Toggling the light intensity of the LED array between 0 and 1 sun results in alternation between OC and maximum power point (MPP) as HC state of the cell string, which is recorded with one image per switch. Guada et al.^[8] as well as Solarzentrum Stuttgart^[7] work with devices that have to be installed into the string to alter the OP of connected PV modules. Koester et al.^[9] used devices in the field to switch from MPP at normal operation to OC by turning off the inverter or MPP tracker, or disconnecting the string via combiner box switches. A similar approach is used by Vukovic et al. modulating the OP of an inverter remotely,^[11] and further by exploiting the automatic IV sweep in modern inverters.^[12] Images recorded during this IV sweep will include images of both OPs, which are defined and subtracted afterward.

In each case, multiple images of each OP are taken in a short time period and then averaged. The images can be recorded either alternating (continuous toggling of OP, taking one image per switch) or using a batched method (one switch to the other OP, taking all images in a row). Alternating image acquisition reduces the impact of changing irradiance during the imaging process, but it requires a very precise synchronization between the camera and the OP switching device, or a postprocessing step to separate images of different OPs, as reported by Alves dos Reis Benatto et al.^[13] Fast switching cannot be performed on PV modules using module-level optimizers.^[14] While most approaches described above use the alternating method, Vukovic et al.^[12] and Koester et al.^[9] used the batched method. To reduce the impact of irradiance alteration during batched imaging, Bhoopathy et al.^[14] introduced intensity correction by comparing an unmodulated area of the recorded images (not active PV module surface, e.g., the ground, a wall in the background, or even the cell gaps in the same PV module). The intensity in this region should be stable toward the changes of OP, and changes reflect alternations in irradiance. If this so-called normalization area (NA) is close to the active area, the signal might be influenced by the luminescence radiation (e.g., reflection on the ground), but to a lesser extent, and therefore intensity correction is still beneficial for OP detection.

In the following, the active module area is called the region of interest (ROI).

2.2. OP Switching-Enabled Inverter

To enable DPL for large-scale PV plant inspection, the OP switching needs to be achievable for all PV modules in a plant with minimum effort. Therefore, in the H2020 project *TRUST-PV*, a *Huawei* smart string inverter was upgraded to perform OP toggling following changeable conditions. Via ModBus control, it is possible to define for each OP the voltage point (with maximum voltage to reach OC and another voltage to choose for setting the HC state) and the toggling time. The solution developed by *Huawei* is a full software solution. Therefore, by updating its firmware, each *Huawei* smart string inverter could be enabled to be DPL-ready. To switch between both OPs, the time for transition varies with different toggling times. For a typically used toggling time of 200 ms (the time, each OP is active before switching), a total transition time of around 5 ms was recorded.

2.3. InGaAs Camera

The luminescence signal of crystalline Si is emitted in the SWIR, with a broad spectrum around 1140 nm at room temperature.^[15] A camera with InGaAs sensor offers high quantum efficiency in this regime, which is important to identify the luminescence signal among the ambient radiation and also for fast imaging in UAV applications. The camera used here is the *OWL640 Mini* by *Raptor Photonics*. It has a resolution of 640×512 pixels and records 16-bit grayscale images with a minimum theoretical exposure time down to $10 \mu\text{s}$ (in practice, 1 ms). To increase the share of luminescence signal in the acquired images, it is equipped with a bandpass filter of central wavelength 1137 nm and full width at half maximum of 25 nm. The read-out noise of the camera is noted with $< 190 e^-$ for a full well capacity of $650 ke^-$.

The intensity measured by the camera, I_{sensor} , is calculated as the average intensity of each pixel within one image. Throughout this work, the recorded intensity is denoted with I , while the

luminescence intensity, as a result of subtracting OC and HC intensities of the image cropped to the ROI, is denoted with Φ .

The ability of the camera sensor to record stable signal intensity within a series of images taken as an image batch was investigated by recording several images of a stable background over time. The development of image intensity, as average of all pixel intensities, is then investigated for the recorded image batch, as shown in **Figure 1**. While the dark noise can be neglected, abrupt changes of up to 2% in intensity are visible. These changes are of unclear origin and therefore 2% is added to the uncertainty of the camera.

3. Semibatched Imaging with Automated OP Detection

For efficient and price-effective DPL imaging, it must be applied using UAVs. This raises two challenges: on the one hand, quick imaging with fast OP switches is crucial. On the other hand, avoiding an active synchronization of OP switching by the inverter and images taken by the camera simplifies the application of DPL in the field.

3.1. Semibatched DPL Imaging

To tackle both challenges, in *TRUST-PV*, along with the DPL-ready inverter, *Eurac Research* developed automated OP detection and the semibatched imaging method to perform DPL. The idea of this method was initially introduced by Alves dos Reis Benatto et al.^[13] It works by switching the OPs with above-described inverter in a fixed time interval, which is several times longer than the exposure time of the camera. While doing so, images are recorded with a frame rate higher than the toggling time of the OP. The OPs for each image are defined in a processing step subsequent to the imaging by comparing the total intensity of the active area in each image relative to each other. The process developed is described in the following sections. The idea of semibatched imaging was initially introduced by Bhoopathy et al.^[16] but with synchronization of camera and LED array.

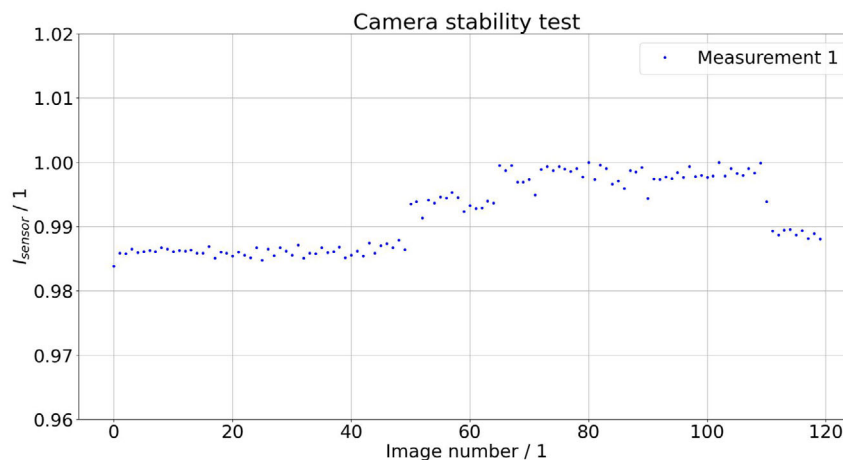


Figure 1. Camera stability test of *OWL640 mini* InGaAs camera. Under constant illumination, the relative recorded intensity I_{sensor} of an image batch of 120 images is recorded with a frame rate of 10 images/second.

3.2. Detection Algorithm

The evolution of I_{ROI} within one image batch includes changes due to irradiance and luminescence by OP switching, the latter to a greater share. Even though it is recommended to perform DPL under stable conditions with minimal changes in irradiance, the impact of small ambient variations is excluded. The intensity of each image in a batch, $I_{ROI,raw,i}$ is normalized by the correction factor defined by the ratio of intensity in the NA in that image, $I_{NA,i}$, compared to the one in the first image of the batch, $I_{NA,0}$. Giving the corrected $I_{ROI,i}$ of that image:

$$I_{ROI,i} = \frac{I_{NA,i}}{I_{NA,0}} \cdot I_{ROI,raw,i} \quad (1)$$

The corrected intensity is now used to define the OP of each image, as notable changes in I_{ROI} can be assigned to OP switching. To do so, the developed algorithm calculates the intensity ratio I_r between I_{ROI} of each image i and its previous image,

$$I_r = \frac{I_{ROI,i}}{I_{ROI,i-1}} \quad (2)$$

For a repetition of the same OP, I_r is close to 1. For an OP switch instead, the deviation of I_r from 1 increases. To detect an OP switch, the threshold h is introduced, as maximum allowed deviation of I_r from 1 for remaining in the same OP. Thus, an OP switch is detected if one of the following conditions is met:

$$I_r < (1 - h) \rightarrow \text{OC to HC switch}$$

$$I_r > (1 + h) \rightarrow \text{HC to OC switch}$$

Values between $(1 - h) < I_r < (1 + h)$ indicate the absence of an OP switch. The actual value of h depends strongly on imaging

conditions like imaging speed and resulting changes between images. A value of h between 0.01 and 0.02 has shown to be reliable for stable irradiance conditions. If, for a chosen h , no OP switches are detected throughout the image batch, the threshold is decreased and the process is repeated. If OPs are detected, their equidistance is verified. If there is a large discrepancy between the number of HC and OC OPs, h needs to be increased. **Figure 2** shows a sample of an image batch with recorded intensities and detected OPs, with the corresponding I_r values.

A luminescence image is consequently determined by averaging all pixels in the images of each OC and HC point separately, followed by a pixel-wise subtraction of HC from OC. For quantitative inspections in this work, the DPL signal intensity Φ_{ROI} of an ROI is given by

$$\Phi_{ROI} = I_{ROI,OC} - I_{ROI,HC} \quad (3)$$

with $I_{ROI,OC}$ and $I_{ROI,HC}$ being the average intensity of the ROI and all images detected for OC and HC, respectively.

3.3. Exclusion of Transition Points

Due to the transition time of the OP in the inverter and depending on the frame rate and exposure time of the camera, it is possible that an image which includes the transition of one OP to the other is recorded. That results in intensity values between HC and OC, visible in Figure 2 as intensity points with $I_{ROI} \in [18000, 20000]$. If these points are assigned to one or the other OP, they falsify the average intensity for this OP. These transition images are excluded from the analysis, identified by comparing the intensity of each image to the neighboring intensities of the same OP. Depending on the threshold chosen,

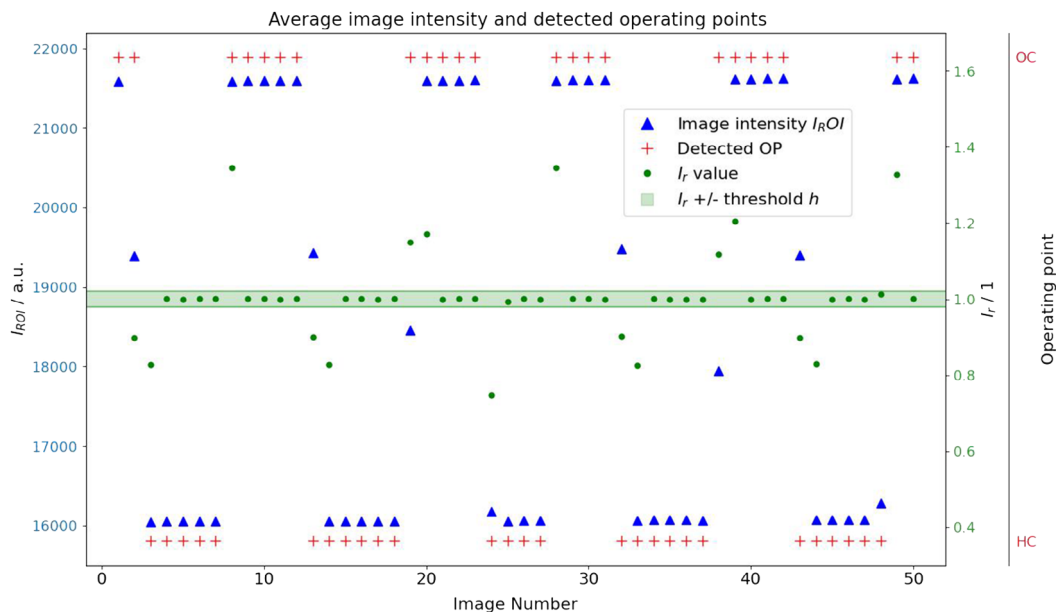


Figure 2. Intensity I_{ROI} of active module area during DPL (blue triangles). OPs detected as described in Section 3.2 (red crosses). Intensity ratio I_r as described in Equation (2) (green dots) with green threshold area defined by $h = 0.02$. Transition points with intermediate intensity located around the center between OC and HC value can occur due to long exposure times. Soft outliers are transition points very close to HC value for images 24 and 48.

also soft outliers, like the one at images 24 and 48 in Figure 2, can be excluded.

For qualitative DPL images, the outliers have no noticeable effect. Nevertheless, strong outliers are excluded. For quantitative analysis, also soft outliers are excluded.

4. Methods and Theory

4.1. Luminescence Signal Intensity and Temperature

DPL uses daylight to excite carriers in the solar cell material of PV modules. Silicon, used for the majority of worldwide installed PV modules, emits photons in the SWIR, in a range peaking around 1140 nm, corresponding to the bandgap energy of silicon (1.12 eV at room temperature).^[17] Although only 1% of the recombination processes in Si result in the release of a detectable photon,^[18] it is enough to detect the signal and investigate it. The luminescence signal intensity Φ_{PL} depends on several parameters:^[15]

$$\Phi_{PL}(T) = C(T) \cdot \exp\left(\frac{qV(T)}{k_B T}\right) + \Phi_{offset} \quad (4)$$

where q is the elementary charge ($-1.60217 \cdot 10^{-19}$ C), k_B ($1.38065 \cdot 10^{-23}$ J K⁻¹) is Boltzmann's constant, and V and T are cell voltage (in Volts) and temperature (in Kelvin), respectively. Φ_{offset} is the luminescence signal created independently of the OP. It arises due to excited carriers which are not able to reach the junction within their lifetime and consequently recombine. As it is comparably small and is canceled out due to the subtraction process of DPL, it will be excluded in the following considerations. $C(T) = C_{opt}B(T)n_i^2(T)$ is the proportionality constant, with C_{opt} taking into account all optical factors of the measurement setup, B is the radiative recombination factor of Si, and n_i is the intrinsic carrier concentration.

While Equation (4) describes the emitted luminescence signal intensity, the intensity recorded by the camera depends on multiple other parameters. To allow quantification and comparison of measured intensities in different conditions, all parameters must be identified and their possible impact analyzed. Changes in the setup or in the ambient conditions can impact either the PL signal intensity itself, the stray (unwanted) radiation, or both at the same time. Factors having an equal impact on both are, for example, the exposure time of the camera which is proportional to the incoming photons. Changing the setup instead can result in a different angle between camera and PV module surface. It can cause a change in the recorded PL signal intensity and the recorded ambient light, but to an unequal share. Therefore, the setup should be mounted the same way if PL intensities, recorded at different times, shall be compared. All identified parameters, affecting part of the recorded signal, are listed in Table 1. The last column indicates, if the specific parameter can and has to be controlled or can be calculated. Controlled means that it must be ensured that the conditions are stable in all measurements done. Determined means instead that the related parameter must be recorded and the PL intensity has to be adjusted accordingly.

Table 1. Parameters influencing the recorded signal intensity. Determination if the change in intensity is due to changes in the ambient signal, the actual PL signal, or both. For quantitative DPL measurements, some parameters have to be controlled and determined.

Changing parameter	Affects PL signal	Affects ambient signal	Possible to control (c) or determine (d)
Camera settings (exposure time, aperture, gain...)	X	X	c
Cell temperature	X	–	d (Equation (9))
Cell V_{OC}	X	–	–
OPs set at inverter	X	–	c
Uncertainty inverter	X	–	–
Orientation camera - sun	–	X	–
Orientation camera - PV module	X	X	c
Irradiance	X	X	d (Equation (7))
Camera stability uncertainty (cf. Section 2.3)	X	X	–

4.1.1. Irradiance and Temperature Dependency

Even though Equation (4) does not show a direct dependence on irradiance, the number of emitted photons through luminescence depends on the free carriers inside the Si material available for recombination and thus, on the amount of generated carriers. The recombination rate R for Si is expressed as:^[19]

$$R = B(np - n_{i,eff}^2) \quad (5)$$

where $n_{i,eff}$ is the effective intrinsic carrier concentration and n and p are the densities of free electrons and holes, respectively. The generation G of these free carriers, depending on distance into the material x , is given by

$$G = \alpha N_0 \exp(-\alpha x) \quad (6)$$

with α being the absorption coefficient and N_0 the photon flux on the surface. Therefore, irradiance must be considered if the luminescence intensity during DPL is investigated. The radiative recombination coefficient B decreases for higher injection densities,^[19] and therefore for increased irradiance. The investigations done in this work are for small irradiance changes, thus B is assumed to be constant. The measured luminescence intensity, Φ_{meas} , corrected to standard test conditions (STC) irradiance of 1000 W m⁻², is given with

$$\Phi_{Gcorr} = \frac{1000}{G_{PoA}} * \Phi_{meas} \quad (7)$$

Here, only the irradiance on the front surface G_{PoA} is considered, as it is assumed that the DPL signal is created mainly in the surface layer of the irradiated Si.

Next to irradiance, cell temperature plays a major role for the luminescence signal intensity. As already emphasized in Equation (4), not only the direct temperature dependency in the equation plays a role, but also the dependency of the other variables on temperature, such as $V(T)$, $B(T)$, and $n_i(T)$.

According to Trupke et al.^[20] the temperature dependency of factor B is minimal around room temperature ($B(249\text{ K}) = 5.48 \cdot 10^{-15}$, $B(300\text{ K}) = 4.73 \cdot 10^{-15}\text{ cm}^3\text{s}^{-1}$). Consequently, it is treated as constant in this study. In Si, n_i shows a strong dependency on temperature^[20]:

$$n_i(T) = 5.29 \cdot 10^{19} \cdot \left(\frac{T}{300}\right)^{2.54} \exp\left(-\frac{6726}{T}\right) \quad (8)$$

While the actual value for a specific Si-cell may vary, in this work, only the relative behavior of the luminescence intensity of the same cell (technology) to each other is considered. Therefore, only the behavior on temperature and not the absolute value of n_i is of importance. The temperature dependency of the cell voltage is given by the temperature coefficient $\beta_{V_{OC}}$, provided in the PV module data sheet. While the product of $C_{opt} \cdot B$ is not provided, it is derived by inserting the given parameters under STC into Equation (4), and then treated as constant. By calculating Φ_{PL} for different temperatures, the trend, and therefore a temperature coefficient of the PL intensity, γ_{PL} , in $\%K^{-1}$, can be derived. This temperature coefficient is used to adjust the measured PL intensity Φ_{meas} of a given temperature T_1 against the STC temperature, $T_{STC} = 298\text{ K}$, resulting in the temperature-corrected PL signal intensity:

$$\Phi_{T_{corr}} = \frac{\Phi_{meas}(T_1)}{\frac{\gamma_{PL}}{100} \cdot (T_1 - T_{STC}) + 1} \quad (9)$$

4.2. Performance Loss Detection with DPL

Although the DPL signal depends on several uncontrollable external parameters, this work analyses the possibility of quantitative DPL image analysis and to identify the impact of changes in V_{OC} in the signal intensity. Therefore, the applicability of the DPL method to detect general performance losses in PV modules and plants is studied using two approaches: 1) Development of Φ_{PL} of the same PV module over time. Taking DPL images over a long time period should make the usual performance decay of a PV module visible. Especially decay in a PV module's V_{OC} results in a significant decrease of Φ_{PL} . To ensure repeatability of OPs, reliable switching between V_{OC} and I_{SC} is necessary, as can be done with DPL-ready inverters. To achieve maximum repeatability, images should be acquired with camera and PV module in the preferably same position. A picture of the setup and markings on

the ground can help in achieving that. Even though changes in irradiance can be calculated, images should be taken ideally during the same time of the day and sun position (depending on the angle, also zenith and therefore season may play a role) to have a comparable orientation between camera and sun. The camera settings have to be the same.

In this work, the repeatability of these measurements is tested by doing several image cycles of a heterojunction technology (HJT) PV module in a string controlled by a DPL-ready inverter. Between each image cycle, all performed in one day, the whole setup is reset: the camera is moved anew into position and the software rebooted. The impact of irradiance is investigated by doing time-delayed image cycles. For each image cycle, three batches are recorded. 2) Comparing Φ_{PL} of PV modules in the same DPL image to each other. Recording a DPL image of multiple PV modules of the same technology in one image allows to intercompare Φ_{PL} of the different PV modules with each other. If there is a difference in PV module voltage, the average of the intensity per module should reflect that. For this approach, the imaging parameters are less important, as the signal does not have to be reproduced. It must be considered though, that the compared PV modules are not in an equal distance to the camera. Therefore, the actual center distance of each PV module is calculated using basic trigonometry. Angle of incidence correction can be performed, considering that the irradiance decreases with the square of the distance between light source (PV module) and illuminated area (camera sensor).

In this work, three passivated emitter and rear cell (PERC) PV modules are installed next to each other. The PV module parameters are measured with a portable IV tracer. All PV modules are of the same type, but during the last 2 years, two of them have been operating outdoors, while the third one was kept in storage. The 2 years of operation should theoretically result in a performance decay, accompanied with a lower V_{OC} . For this measurement, the DPL image is recorded in full batched method, by switching off the inverter and forcing the connected PV modules from MPP to OC condition. This process is repeated several times for different distances between camera and modules. An example image of this setup is shown in **Figure 3**, with ROIs of the three PV modules and a possible NA. This graph also depicts the averaging over HC and OC images and shows the resulting DPL image due to subtraction.

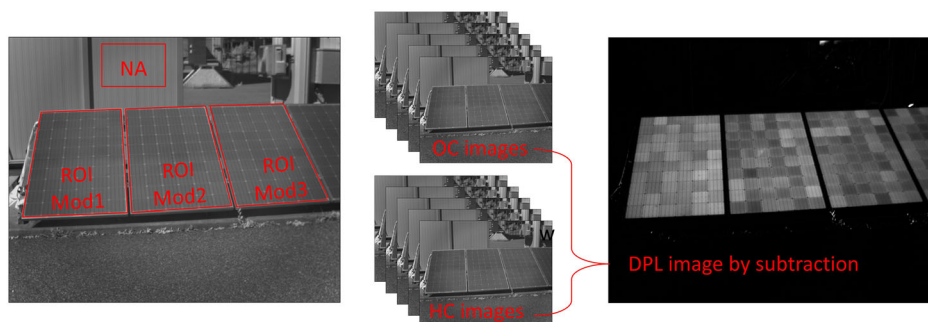


Figure 3. DPL image of three PV modules with differently progressed degradation. HC image with NA and ROIs visualized by red frames (left). Subtraction process of averages between OC and HC images (center) leads to DPL image (right). The least-degraded PV module is the one on the left, progressed degradation in the other two modules also visible by increased mismatch between cells.

5. Results and Discussion

In this section, the results of the experiments conducted are evaluated. First, a sensitivity analysis of the temperature dependency of DPL intensity as described in Section 4.1.1 is given. In the second part, the focus shifts to the two approaches concerning performance loss detection.

5.1. Sensitivity Analysis of DPL Intensity

A sensitivity analysis of the various parameters impacting the DPL intensity is conducted, evaluating the dependency with respect to temperature. While n_i^2 substantially influences the intensity magnitude, its effect on temperature behavior is limited. In contrast, voltage and temperature individually have an exponential influence on DPL intensity. Two PV module types (HJT and PERC) are investigated within this work, with cell voltages of $V_{OC,HJT} = 0.731$ V and $V_{OC,PERC} = 0.663$ V. The temperature coefficients are derived by Equation (4) as described in Section 4.1, using the corresponding $\beta_{V_{OC}}$ of the two investigated PV modules and applying a linear fit to the result. The trends for different cell voltages are shown in Figure 4. This gives $\gamma_{PL,HJT} = -0.63\% K^{-1}$ and $\gamma_{PL,PERC} = 0.81\% K^{-1}$. $\gamma_{PL,HJT}$ aligns with the experimental findings from Ref. [9]. The higher cell voltage resulting in a negative temperature dependency of the luminescence signal intensity is not in line with findings by Zafirovska et al.^[21] who show a negative temperature coefficient, independently of the cell voltage. An experimental verification of the findings in this work is still pending for future work.

5.2. Performance-Related Intensity Decrease Over Time

During one clear-sky day, five cycles of each three batches of images were recorded. Between each cycle, the equipment was newly set up and for each cycle three batches were recorded within 2 min. Between Cycle 1 to 4, a break of around 15 min was kept to allow for changes in irradiance. Cycle 4 and 5 were recorded with only 2 min delay in between to maintain a comparable irradiance. Table 2 shows irradiance values measured with

Table 2. Irradiance of measurements performed and shown in Figure 5. Recorded values were stable over the measurement time within a range of ± 2 W m⁻².

Cycle	Irradiance in W m ⁻²			
	Batch 1	Batch 2	Batch 3	Batch 4
1	635	630	625	
2	562	558	554	
3	504	500	496	490
4	427	423	421	
5	411	408	404	

a permanently installed pyranometer on the test-site. The temporal resolution of this pyranometer is 10 s, which leads to a possible delay between irradiance measurement and DPL image taken of max 5 s. The irradiance during that time and the whole batch measurement was recorded with a portable pyranometer with one second temporal resolution, only images with variations below ± 2 W m⁻² throughout the measurement are considered. Within one batch, no irradiance correction could be performed for single images. Images are recorded with an exposure time of 4 ms. To confirm the linear dependency of signal intensity to exposure time, a fourth measurement is performed in Cycle 3, with exposure time decreased to 2 ms, thus half of the one during the other measurements.

The DPL intensity is calculated for an ROI of one individual cell of the PV module, to avoid including of nonmodulated cell gaps. The luminescence intensity of all measurements is normalized to the maximum one recorded to show their relative behavior. Figure 5a shows Φ_{rel} of the intensities measured, including the error due to uncertainty of the camera, and Figure 5b shows the irradiance and temperature corrected values of Φ_{rel} , following Equation (7) and (9), respectively, including error bars for the uncertainty of the camera, temperature sensor, and pyranometer. Measurement 16 is the fourth batch done in Cycle 3, where the exposure time is reduced to two instead of 4 milliseconds, but with a correction following the assumption that exposure time is linear to photon capture.^[18] Therefore, the measured intensity is doubled

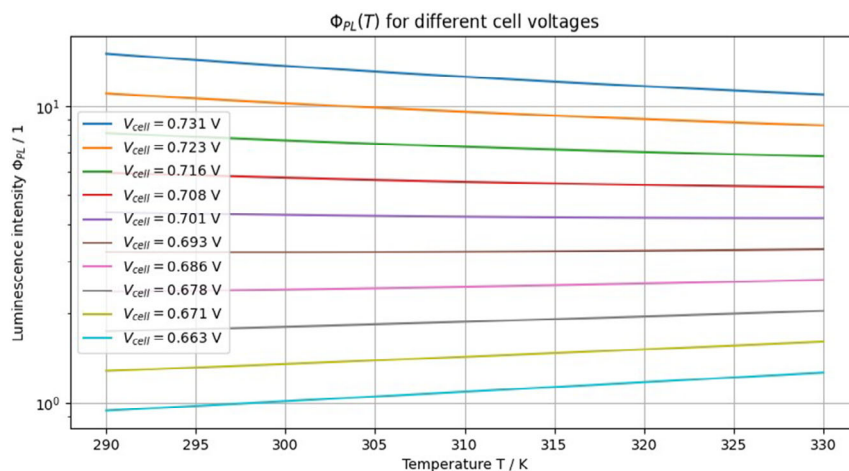


Figure 4. Behavior of $\Phi_{PL}(T)$ for different cell voltages (other parameters kept constant).

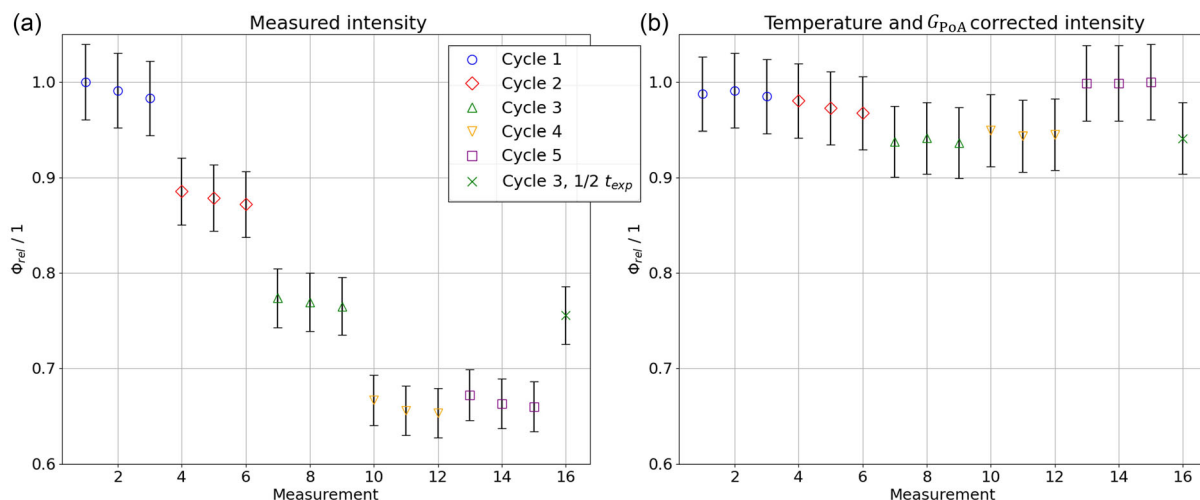


Figure 5. Repeatability of luminescence intensity of same module (cell) over time. Five imaging rounds of each three image batches. a) Raw measured intensities and b) temperature and irradiance corrected intensities. Measurement 16 is recorded with an exposure time of 2 ms, compared to 4 ms for all other measurements, but the value shown is double of the measured one to account for less captured photons.

for this measurement and the intensity shown of Measurement 16 in Figure 5 is the corrected one. Besides the reduced signal intensity for different irradiances, there are no visible differences in the quality of the final DPL images. It should be considered, that for very low irradiances around 100 W m^{-2} , the influence of shunt resistance becomes dominant and DPL images look like EL images with 10% short-circuit current injection.^[22]

Overall, the measurements show a variation of about 6%, even after the correction of temperature and irradiance. The aim of this work was to show that the same result can be achieved between different measurements, within the uncertainties given. Due to the relatively strong uncertainty by camera stability and other sensors, all measurements lie within each other's error bars. That, in turn, means only strong degradation and resulting variations in Φ_{PL} can be reliably detected, but small differences in Φ_{PL} , induced due to degradation in V_{OC} , might be masked by the uncertainty. This is the case for comparing single measurements; nevertheless, if this measurement is conducted regularly, a trend in Φ_{PL} may become apparent.

5.3. Intensity Comparison within One Image

Three PERC PV modules (Mod1, Mod2, and Mod3) are mounted next to each other and connected to the same inverter. For each PV module, the OC voltage is measured (Mod1: $V_{OC,cell} = 0.656 \text{ V}$; Mod2: $V_{OC,cell} = 0.650 \text{ V}$; Mod3: $V_{OC,cell} = 0.650 \text{ V}$). Three DPL images are recorded in different occasions from the same distance, capturing all three PV modules in the image frame. For each module individually, and each image batch respectively, the DPL intensity is calculated as average of the whole module ROI and corrected toward angle of incidence. The resulting DPL image is shown in Figure 3, with the frames depicting the ROIs of each PV module, separately.

For each image, Mod1 shows the maximum DPL intensity. To allow comparison of the different measurements in the same graph, the intensities of all modules are normalized to the

maximum Φ_{PL} in each image, giving Φ_{rel} . According to Equation (4), $\Phi_{rel}(V)$ is calculated using the DPL intensity of Mod1 and its cell V_{OC} . The black line in Figure 6 shows the resulting function. The graph shows for each measurement $\Phi_{rel}(Mod1) = 1$ due to the normalization, and the results of Mod2 and Mod3 are in relation to it, with their respective cell V_{OC} at STC. The error bars of cell voltage are given via the uncertainty of the IV tracer, the ones for DPL intensity by the camera signal instability.

Mod1, with the highest cell voltage, shows for all measurements the highest PL intensity, as expected. The other two PV modules show a lower PL intensity, in line with the expectations due to their degraded V_{OC} . The high uncertainty of the measured voltage for each PV module combined with the strong sensibility of PL signal intensity on the voltage prevents a precise alignment of the experimental results to the modeled one. More results with further degraded PV modules are needed to give a statistical meaningful number of results with a trend to recompile the modeled curve. Nevertheless, considering the voltage uncertainty, all other measurements are in an expected distance toward calculated $\Phi_{rel}(V)$. Nevertheless, the relative luminescence intensity of the other two modules is slightly different, although their cell V_{OC} at STC is the same. In Measurement 3, Mod3 shows a relative signal about 10% less compared to the previous measurements, which must be classified as an outlier. Further, due to different conditions of the measurements, and slight variation of the camera position in relation to the PV modules and sun position, changes in irradiance, sun movement and resulting variations in reflection on the PV modules surfaces, can cause uncontrollable effects. Even though most of these effects should have been eliminated due to the subtraction process of DPL, the unequal orientation of the three modules toward the camera can cause an uneven effect, as described in Section 4.1. But even with all these effects considered, the deviation of PL intensity measurements including error bars results in a smaller range of corresponding voltage in comparison to the voltage measurements done with the IV tracer. Therefore, it can be concluded that a

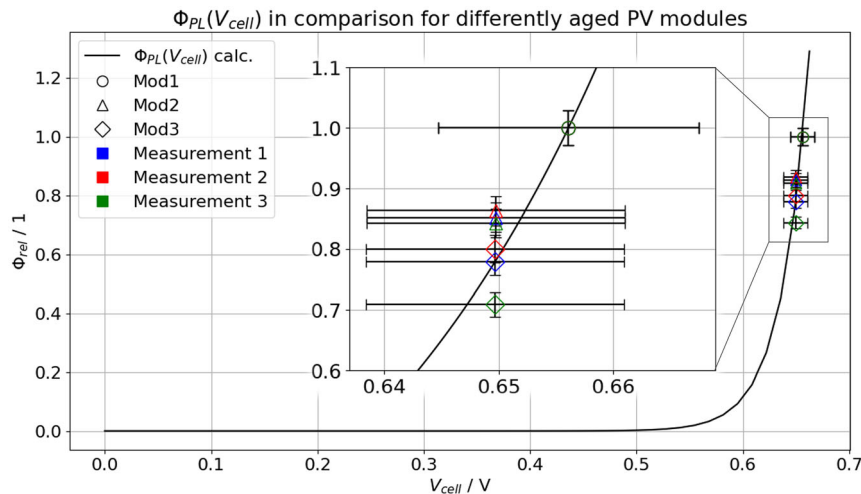


Figure 6. DPL intensity to cell voltage for three PERC PV modules with different V_{OC} . The black line indicates the expected DPL intensity according to Equation (4), with $\Phi_{rel}(\text{Mod1})$ and cell $V_{OC}(\text{Mod1})$. Different colors indicate three separately taken DPL images with Mod1 always producing the maximum intensity.

voltage measurement with DPL can be more precise than a voltage measurement using the PV modules terminals. This aligns with the findings by Zafirovska et al.^[21] showing the higher sensitivity toward temperature of terminal voltage measurements compared to voltage measurements by EL or PL techniques.

6. Conclusion and Outlook

In this work, the application of DPL for identifying power losses in PV modules is evaluated. DPL is a novel inspection method, only used for qualitative PV module inspection so far. To make it a cost-efficient inspection method for large-scale PV installations, imaging speed is a crucial factor. The time-consuming process of connecting additional hardware to enable OP toggling can be overcome by the DPL-ready inverter presented in this work. Further, to enable UAV-based inspection, the semibatched imaging method with automated OP detection in a processing step postimaging is presented. While OP detection works reliable, the exclusion of transition points must be included, if a quantitative DPL image analysis is intended instead of qualitative one. The actual demonstration of DPL imaging on an UAV is still pending.

To investigate accurately the DPL image intensity and exploit it for quantitative measurements, all impacting factors must be considered carefully. The different factors are defined in this work and the impact of temperature on the signal intensity is investigated. The DPL intensity temperature coefficient for a HJT module with high cell voltage is calculated with $\gamma_{PL,HJT} = -0.63\% K^{-1}$, which confirms the experimentally derived value from previous work. For lower cell voltages, the temperature coefficient shows an opposite behavior, which is contrary to published literature and has to be investigated further.

To use quantitative DPL images for analyzing performance degradation of PV modules, two approaches are followed and presented in this work.

The possibility of comparing the DPL intensity measured periodically over long time periods is approached by proving that the

same DPL signal under changing conditions in short time periods can be measured, where no degradation is expected. Although we have demonstrated this, the relatively high uncertainty range for the measurements indicates that only very strong degradation and resulting variations in Φ_{PL} can be reliably detected, and the expected small differences in Φ_{PL} , induced due to degradation in V_{OC} , will be hidden within the measurement uncertainty. This is the case for comparing single measurements, nevertheless, if this measurement is conducted regularly, a trend in Φ_{PL} will likely become visible. This will be controlled and examined in future work. Also, the impact of albedo on the DPL signal intensity will be examined.

In the second approach, the effect of V_{OC} degradation on the DPL intensity is investigated by comparing differently aged PV modules of the same type next to each other within one DPL image. The PV modules with lower voltage show a significantly decreased luminescence intensity. The relative intensity difference in images achieved under changed ambient conditions varies, although mostly within the given uncertainty. Future work needs to investigate it further and verify the reliability of this inspection by applying it on more samples. These results show that the voltage measurement with DPL has the possibility to offer a higher precision than a voltage measurement with common equipment, like an IV tracer.

In summary, this work presents a positive first approach on tackling quantitative DPL imaging to detect performance degradation of PV modules. The reliability of these measurements will be shown in long-term measurements.

Acknowledgements

The authors would like to thank the Power Conversion Technology Laboratory of Huawei Nuremberg Research Center for the collaboration within TRUST-PV and for developing the daylight photoluminescence-ready inverter.

The work was supported by funding from the European Union's Horizon 2020 Research and Innovation Programme under grant agreement N952957, project "TRUST-PV".

Conflict of Interest

The authors declare no conflict of interest.

Data Availability Statement

The data that support the findings of this study are available from the corresponding author upon reasonable request.

Keywords

daylight photoluminescence, degradation detection, performance

Received: August 25, 2023

Revised: November 6, 2023

Published online: November 23, 2023

- [1] IEC62446-3, *Photovoltaic (PV) systems - Requirements for testing, documentation and maintenance - Part 3: Photovoltaic modules and plants - Outdoor infrared thermography*. Technical Specification IEC TS 62446-3:2017. International Electrotechnical Commission, Geneva, CH **2017**.
- [2] IEC TS 60904-13, *Photovoltaic Devices - Part 13: Electroluminescence of Photovoltaic Modules*. Technical Specification. International Electrotechnical Commission (IEC), Geneva, CH **2018**.
- [3] L. Koester, E. Vallarella, A. Louwen, S. Lindig, D. Moser, *EPJ Photovolt.* **2023**, 14, 12.
- [4] A. Ara, A. Lee, A. Sacco, A. Rahmati, A. Finch, B. Jäckel, C. Fergus, C. Voet, C. Peonides, D. Moser, D. Ioushua, E. Teo, E. Tilly, F. Stüwe, G. Hilti, I. Tsanakas, J. G. Jensen, J. Brajkovic, J. Althaus, N. Mutch, P. Van der Stock, R. Gottschalg, R. Chervier, R. Lowry, R. Andrews, R. Taylor, T. Lebreuilly, T. Moeller, V. Giorgio, W. Hitchcock, et al., *Operation & Maintenance - Best practice guidelines*. en. Best practice guidelines Version 5.0. Solar Power Europe, December **2021**.
- [5] W. Herrmann, G. Eder, B. Farnung, G. Friesen, M. Köntges, B. Kubicek, O. Kunz, H. Liu, D. Parlevliet, I. Tsanakas, J. Vedde, *IEA-PVPS Task 13: Performance, Operation and Reliability of Photovoltaic Systems – Qualification of Photovoltaic (PV) Power Plants using Mobile Test Equipment, Report*. International Energy Agency **2021**.
- [6] R. Bhoopathy, O. Kunz, M. Juhl, T. Trupke, Z. Hameiri, *Prog. Photovolt.: Res. Appl.* **2018**, 26, 69.
- [7] Solarzentrum Stuttgart GmbH, *Daysy - Daylight Luminescence System - Measurement Guide*, https://www.solarzentrum-stuttgart.com/uploads/file/DaySy_Measurement_Guide_current.pdf, **2019** (accessed: October 2021).
- [8] M. Guada, A. Moreton, S. Rodriguez-Conde, L. A. Sanchez, M. Martinez, M. A. Gonzalez, J. Jimenez, L. Perez, V. Parra, O. Martinez, *Energy Sci. Eng.* **2020**, 1, <https://doi.org/10.1002/ese3.781>.
- [9] L. Koester, A. Astigarraga, S. Lindig, D. Moser, in *37th EU-PVSEC. 37th EUPVSEC* **2020**, p. 6, <https://doi.org/10.4229/EUPVSEC20202020-4CO.4.2>.
- [10] L. Stoicescu, M. Reuter, J. H. Werner, in *29th EUPVSEC*, Amsterdam, Netherlands **2014**, pp. 2553–2554.
- [11] M. Vuković, I. Eriksdatter Høiaas, M. Jakovljević, A. Svarstad Flø, E. Olsen, I. Burud, *Prog. Photovolt.: Res. Appl.* **2022**, 30, 436.
- [12] M. Vukovic, M. Jakovljevic, A. Flø, E. Olsen, I. Burud, *Appl. Phys. Lett.* **2022**, 120, <https://doi.org/10.1063/5.0097576>.
- [13] G. A. dos Reis Benatto, C. Mantel, S. Spataru, A. A. Santamaria Lancia, N. Riedel, S. Thorsteinsson, P. B. Poulsen, H. Parikh, S. Forchhammer, D. Sera, *IEEE J. Photovolt.* **2020**, 10, 872.
- [14] R. Bhoopathy, O. Kunz, M. Juhl, T. Trupke, Z. Hameiri, *Prog. Photovolt.: Res. Appl.* **2019**, <https://doi.org/10.1002/pip.3216>.
- [15] T. Trupke, B. Mitchell, J. W. Weber, W. McMillan, R. A. Bardos, R. Kroeze, *Energy Procedia* **2012**, 15, 135.
- [16] R. Bhoopathy, O. Kunz, R. W. Dumbrell, T. Trupke, Z. Hameiri, *IEEE J. Photovolt.* **2021**, 11, 164.
- [17] A. Reinders, P. Verlinden, V. W. Sark, A. Freundlich, Eds. *Photovoltaic Solar Energy: From Fundamentals to Applications*. Chichester, West Sussex, United Kingdom, Hoboken, NJ: John Wiley & Sons Ltd, **2017**. ISBN: 978-1-118-92746-5.
- [18] C. Shen. Power loss analysis via photoluminescence. PhD. UNSW Australia, June **2014**.
- [19] P. P. Altermatt, F. Geelhaar, T. Trupke, X. Dai, A. Neisser, E. Daub, *Appl. Phys. Lett.* **2006**, 88, 261901.
- [20] T. Trupke, M. A. Green, P. Würfel, P. P. Altermatt, A. Wang, J. Zhao, R. Corkish, *J. Appl. Phys.* **2003**, 94, 4930.
- [21] I. Zafirovska, M. K. Juhl, A. Ciesla, R. Evans, T. Trupke, *Sol. Energy Mater. Sol. Cells* **2019**, 199, 50.
- [22] M. Vuković, M. Hillestad, M. Jakovljević, A. S. Flø, E. Olsen, I. Burud, *J. Appl. Phys.* **2023**, 134, 074903.